An Edge Detection Algorithm for Classification Spectral Nonlinear images

Murali Krishna Nagiripati[1], Bullarao Domathoti[2], Nageswara Rao Putta[3]
[1, 2, 3] Department of CSE
[1, 2, 3] Swetha Institute of Technology &Science, Tirupati , AP, INDIA

Abstract- *Two model-based algorithms for edge detection in spectral imagery are developed that primarily target shooting intrinsic facets akin to isoluminant edges which are characterised via a bounce in colour however no longer in depth. Given prior capabilities of the courses of reflectance or remittance spectra related to candidate objects in a scene, a small set of spectral-band ratios, which most profoundly establish the edge between each and every pair of materials, are chosen to define a area signature. The bands that type the threshold signature are fed right into a spatial mask, producing a sparse joint spatiospectral nonlinear operator. The first algorithm achieves side detection for every fabric pair by means of matching the response of the operator at each pixel with the threshold signature for the pair of materials. The second algorithms a classifier-enhanced extension of the first algorithm that adaptively accentuates unusual elements earlier than making use of the spatial spectral operator. Both algorithms are commonly tested making use of spectral imagery from the airborne hyper spectral imager and from a dots-in-a-well mid infrared imager. In both cases, the multicolor gradient (MCG) and the hyper spectral/spatial detection of edges (HySPADE) aspect detectors are used as a benchmark for assessment. The outcome display that the proposed algorithms outperform the MCG and HySPADE facet detectors in accuracy, specially when isoluminant edges are gift. Via requiring just a few bands as input to the spatial spectral operator, the algorithms allow tremendous phases of information compression in band selection. Within the offered examples, the specified operations per pixel are lowered by way of a aspect of seventy one with appreciate to those required by using the MCG part detector.*

Keywords- Edge detection, Classification, spectral lengths, Spectral ratio.

I. INTRODUCTION

A spectral imager captures the energy spectral density of light as a perform of wavelength λ and spatial vicinity (x, y). In other phrases, it acquires a 3-dimensional (3D) information cube of knowledge, (x, y; λ), about the scene being imaged. Advantage of the spectral content at quite a lot of spatial areas will also be valuable in picking the composition and structure of objects within the scene being discovered by means of the spectral imager. It is original and conventional for most spectral imagers to accumulate this type of spatio-spectral data dice via temporal scanning both spectrally or spatially.1–3 even as temporal scanning is suitable for spectral imaging of a static scene, it complicates and boundaries the next image processing and analysis for a dynamic scene due to the artifacts caused via the temporal overlap of the scanning operation of the spectral imager with dynamic changes within the scene. In contrast, a image spectral imager eliminates such temporal overlap. In Coded Aperture snapshot Spectral Imagers (CASSI),4, 5 the 3D spatio-spectral know-how a couple of scene of interest is first encoded and received with one photograph on the two-dimensional (second) detector array.

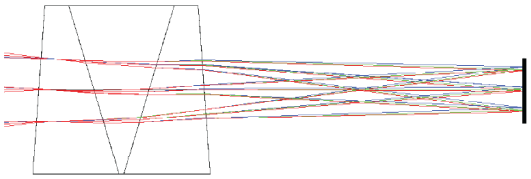

Fig.1: Ray bundles passing through the double Amici prism.

An estimate of the 3D information cube is then acquired by decoding the 2d array of measurements with numerical estimation techniques. In encoding the 3D information right into a second representation, a CASSI system makes use of a coded aperture and one or extra dispersive elements to modulate the optical field from a scene. Right here, we are mainly keen on the one disperser CASSI (SD-CASSI).Four It makes use of an purpose lens to picture the scene on to the aperture of a coded aperture spectrometer.6 In essence, the SD-CASSI extends the utility of the coded aperture spectrometer to coded aperture spectral imaging.

In decoding, the gradient projection for sparse reconstruction (GPSR) procedure was once used in earlier work to estimate the information cube, situated on the assumption that the data dice had a sparse representation in a wavelet groundwork.Four on this paper, we report on replacement approaches for estimating the spatio-spectral knowledge from a 2nd snapshot SD-CASSI detector size. The relaxation of the paper is prepared as follows. Within the next section, we describe a unique SD-CASSI prototype, and the

discretization of a simple mathematical model for mild propagation via the instrument. In section three, we describe the method of calibrating SD-CASSI with a view to provide picture estimation algorithms with a process-specific mannequin that additionally bills for further motives which can be absent in the simplified mild propogation mannequin. In section 4, we describe three spectral image estimation algorithms. In part 5, we present our feedback on experimental results generated by way of the estimation algorithms on experimental information. Part 6 concludes the paper.

The flexibility furnished through the DWELL FPA is just not with out a price, however. For example, the DWELL's spectral Response is relatively huge (≈ 1 − 2m). Hence, the spectral bands similar to special bias voltages showcase tremendous overlap. An additional complication is bias-dependence of the noise (dark current) in the photocurrents. In our previous works we specific addressing each of those challenges. In particular, the DWELL-centered algorithmic spectrometer (DAS), proposed in [8] and validated in [9], [10], banks on utilizing linear superposition of bias-tunable bands of the DWELL person detector to diminish the influence of excessive correlation within the DWELL's bands in the presence of noise achieve target spectrum reconstruction. Figure 1 (b) indicates sequence of synthesized filters (solid traces) which approximate ultimate tuning filters (dashed traces) in the projection stage of the DAS. The full width half of highest (FWHM) of the synthesized filters is 0:threem.

An extra example is the canonical correlation feature resolution (CCFS) algorithm, said in [11], [12]. This algorithm addresses the difficulty of linear superposition of bias-tunable DWELL bands to participate in spectral feature selection (for material classification) founded on spectral matched filtering. Our prior work [11] additionally involves triumphant demonstration of MS classification capability of the DWELL detector, at a single-pixel degree, in phrases of rock-style classification. The be taught was once carried out utilising laboratory spectral knowledge for the rock forms and spectral responsivities measurements of the DWELL detector.

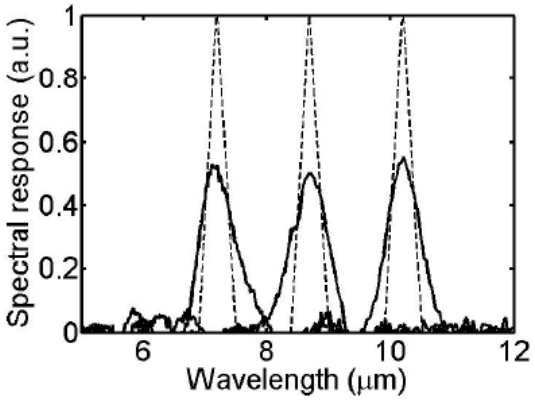

II. THE DWELL FOCAL AIRPLANE ARRAY

On this part we in short describe the operation precept, II. Characterization and bias-stylish spectral tunability of the DWELL FPA.

A. Operation principle and spectral characterization of the DWELL FPA

The DWELL photodetector, pioneered by using S. Krishna [13], is a hybrid variant of quantum dot (QD) and quantum good (QW) photodetectors. The DWELL photodetector said in [9] has already been shown to exhibit bias tunability in the variety of MWIR (3-5 m) to the LWIR (eight-12 m) parts of the spectrum. Most of the time, the MWIR response is driven through a sure-to-continuum transition even as the LWIR is pushed by way of the sure state in the dot-to-a-certain state in the good transition, as shown in Fig. 2. In addition, the asymmetry of the digital capabilities managed by way of the form of the dot and the one-of-a-kind thicknesses of QW above and below the dot, outcome in variant of the nearby talents as a perform of the utilized bias. For that reason, by means of adjusting the utilized bias voltage on the gadget, spectral shift (called additionally "red shift") and overlaps are got, above all in LWIR (eight-12 m) vicinity.

The spectral responses of the single-pixel DWELL shown in Fig. 3 show bias-based spectral tunability for various gadget operating temperatures. The details of the gadget characterization had been said in [9]. The DWELL has been fabricated into a 320 by using 256 detector array layout and is used for this be taught. The fabrication approach is described in pleasant element in [14], [15]. The DWELL FPA responses have been characterized by way of utilising CamIRa demonstration system1.

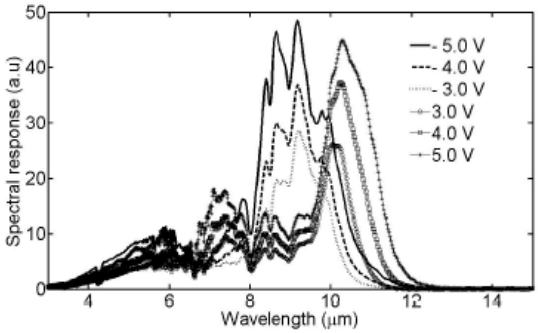

Not too long ago, an optimized DWELL FPA used to be suggested in [14] demonstrating an increase within the running temperature (up to 80 okay) and smaller noise an identical change in temperature (min. NEDT2 round 78 mK). The higher working temperature has been done with the aid of a stress discount and an increased quantity of stacks within the

active vicinity, bettering the responsivity and the absorption quantum effectivity.

B. Bias tunability of the DWELL FPA

DWELL FPA imagery proven in Fig. Four (a-d) are used to show the DWELL FPA bias tunability. For all imagery, the working temperature of the DWELL FPA used to be set to 60 k and the combination (exposure) time used to be eleven.5 ms. The snap shots shown in columns one, three and five in Fig. Four (a–d) are taken at 0.3 V, 0.7 V and 1.2 V, respectively. Normalized pics at zero.3 V, 0.7 V and 1.2 V are shown in columns two, 4 and six respectively in Fig. Four (a–d). The DWELL FPA knowledge is normalized at every pixel by the approximate area of the multibias pixel response as a way to eliminate the depth influence within the calculations. Extra details about the normalization are given in section III. Figure 4 (a-c) contains photographs of distinct configurations of three IR optical filters, manufactured with the aid of Northumbria Optical Coatings Ltd. The spectral responses of the filters are shown in Fig. 5 (left).

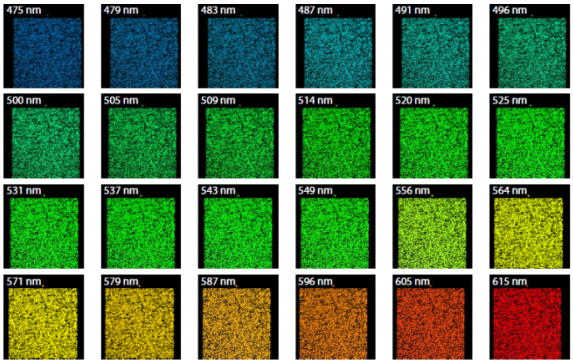

Fig.4. photographs of distinct configurations of three IR optical filters

The first scene, shown in Fig. 4 (a) includes two IR filters: filter at three-4 m termed MW1, filter at four-5 m termed MW2, metal filter holders, and a blackbody history at 150oC. A 150oC temperature was once used given that such a excessive temperature blackbody offered a good transmittance for objects in a scene. The blackbody is manufactured through MIKRON corporation (mannequin M315) supplying a temperature between ambient 5oC and 350oC, a manipulate to inside zero:2oC and an emissivity of +0.Ninety nine. The 2d scene proven in Fig. 4 (b) consists of two filters: MW2 and filter at 8.5 m termed LW3, the equal metallic filter holders and the uniform historical past on the identical temperature.

The third scene in Fig. 4 (c) consists of all three filters MW1, MW2 and LW3 and the background. The scene in Fig. 4 (d) includes two rocks: granite and limestone, and the MW2 filter. Granite is a original and largely occurring sort of intrusive, felsic igneous rock. Granites frequently have a medium to coarse grained texture. Limestone is a sedimentary rock composed generally of the minerals calcite and aragonite, which are one of a kind crystal forms of calcium carbonate. Hornfels is a nice-grained nonfoliated metamorphic rock and not using a designated composition. It is produced via contact metamorphism. Normalized reflectance measurements of granite, limestone and hornfels using a broadband single pixel HgCdTe gadget cooled to 77K are shown in Fig. 5 (proper).

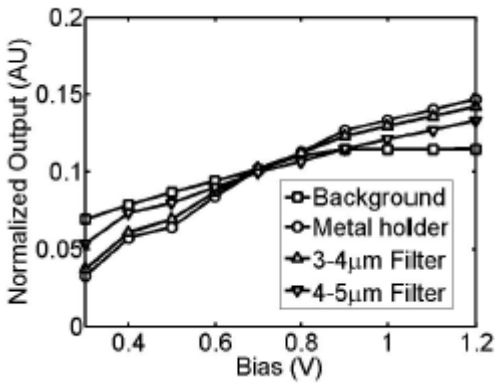

Fig.5: Left: spectral responses of the three IR optical filters:

III. MANNEQUIN DISCRETIZATION

Mannequin discretization has the major function of linking the light propagation model in steady kind to the design of approach calibration quantities and numerical reconstruction models in discrete and finite representations. In spatial discretization, we're concerned no longer best with the pixelation at the detector, but also the spatial modulation of the spatio-spectral vigour spectral density on the coded aperture. The aperture sample T(x, y) is designed as an array of square facets, with each characteristic having a part size qΔ, an indispensable more than one of the detector pixel measurement. Let t(i, j) represent the binary worth on the (i, j)th feature, with a 1 representing an open code feature and a 0 representing a closed code function. Then, T(x, y) can be described.

Classification problems

The primary classification problem viewed in this paper is that of setting apart a couple of combinations of MW and LW IR spectral filters with one-of-a-kind bandwidths and middle wavelengths. For this main issue we used the three scenes shown in Fig. 4 (a-c). The second classification difficulty is to discriminate between pairs of rocks drawn from a set of three special rock varieties: granite, hornfels and limestone. The scene configurations for this main issue are proven in Fig. Four (d) and Fig. 9 left. The classes identified for each classification problems are summarized in table I.

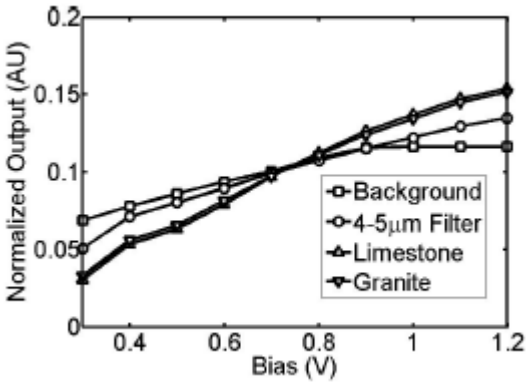

Fig. 9 left. The classes identified for each classification.

Table.1: The classes identified for each classification.

Filter classification problem	Identified classes
Scene (a)	MW_1, MW_2 filters, metal holder and background
Scene (b)	MW_2, LW_3 filters, metal holder and background
Scene (c)	MW_1, MW_2 and LW_3 filters and background
Rock classification problem	**Identified classes**
Scene (a)	MW_2 filter, limestone, granite and background
Scene (b)	granite, hornfels and background

Two varieties of normalization systems are applied to the raw digital numbers (DNs) that are retrieved immediately from the DWELL FPA. First, at each and every bias voltage, pixel's DN values are radiometrically corrected by way of a two-point nonuniformity correction (NUC) algorithm. The NUC compensates for the spatially nonuniform response of the detectors within the FPA [16] and is an integrated part of the snapshot acquisition approach.

The 2-point NUC is performed utilising temperatures at 22oCand 150oC. The shrink temperature of 22oC corresponds to the lens-cap's room temperature, which was used to yield the lower-temperature uniform area. Next, for every radiometrically corrected pixel and its replicas at every bias voltage, the pixel's worth is normalized as follows:

$$I(v_j) = I(v_j) / \Delta v \sum_{Ni=1} I(v_i) \; ; \quad (3)$$

where Δv is the voltage step size used to increment the DWELL FPA's bias. Equation (3) is equivalent to normalization through the area enclosed below the multi-bias response of each and every pixel within the DWELL FPA. The normalized multi-bias response of a pixel can then be written as

$$I = (I(v_1) \; ; \; . \; . \; . \; . \; ; \; I(v_N)) \; ; \quad (4)$$

This normalization minimizes the role of broadband emissivity within the discrimination method and emphasizes the spectral distinction. The normalized snap shots at zero.3, zero.7 and 1.2 V for each classification problems are shown in columns two, four and six in Fig. Four, (a-d) and in Fig. 9 (left), respectively. We participate in a supervised classification comprising of training and checking out steps for each classification problems. To examine representative multi-bias signatures for each type listed in desk I we follow the identical technique as used in [11]. Above all, for every class we compute statistical imply and covariance matrix making use of spatially uniform areas which are visually related to that class. Subsequently, Euclideanand Mahalanobis distance classifiers are proficient via the lessons' imply multi-bias signatures and the covariance matrices [17].

On the trying out step, the expert classifiers are used to classify the objects in table I from a collection of testing scenes. These scenes seize the same pix as the learning scenes but have been obtained at extraordinary occasions. Accordingly, the testing scenes raise inherent variability within the data because of the difference within the measurement stipulations from everyday and the presence of ambient and approach noise. The trying out pix are normalized within the identical fashion as the learning graphics. The dimensions of coaching and checking out data set for the filter and rock classification issues are listed in desk II.

Filter classification problem	Number of pixels in training /testing sets
Scene (a)	MW_1: 140/235, MW_2: 140/235, metal holder: 66/161, background:300/300
Scene (b)	MW_2: 154/330, LW_3: 108/320, metal holder: 126/260, background: 352/340
Scene (c)	MW_1: 400/280, MW_2: 400/280, LW_3 : 400/280, background: 336/350
Rock classification problem	**Number of pixels in training /testing sets**
Scene (a)	granite: 340/420, limestone: 360/450, MW_2: 360/300, background: 336/400
Scene (b)	granite: 224/526, hornfels: 308/870, background: 300/300

IV. DISCUSSION OF THE RESULTS

A. Classification results

The thematic maps for the filter and rock classification issues utilizing Euclidean-distance classifier are presented Figures eight (a-d) and 9, respectively. These maps show the distribution of the derived courses over the spatial discipline captured with the aid of the DWELL FPA. Every map defines a partitioning of the discipline into units, every together with the elements with identical class labels. As a way to investigate the outcomes of the bias choice on the classification accuracy, the classification is performed for multiple mixtures of biases.

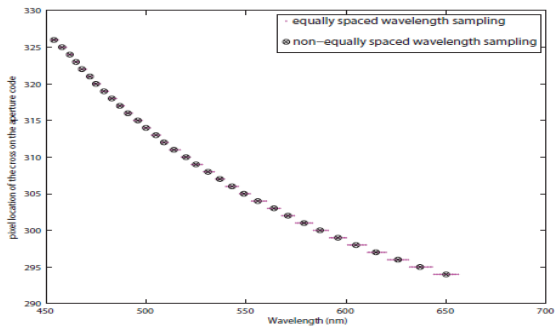

The results for the filter classification concern, distinct in table I, are proven in Fig. Eight (a-c), and desk III indicates the calculated classification blunders per more than a few classification. The thematic maps in Fig. 8 (a-c) are received utilizing four one-of-a-kind sets of bias voltages: (i) one bias at 0.Three V; (ii) one bias at zero.7 V; (iii) two biases at zero.6 V and zero.7 V; (iv) all biases in the range of zero.Three V to 1.2 V. For the first bias voltage set, the Euclidean-distance classifier constantly indicates excellent classification for all three scenes as proven by way of the thematic maps within the first column, (a-c) in Fig. 8. This commentary is established by using the classification blunders in table III for this case. In distinction, for the 2nd bias voltage set the Euclidean-distance classifier can't discriminate efficaciously between the filters, metal holders and background, as proven by using the thematic maps within the 2nd column, (a-c) in Fig. Eight. This influence and the classification blunders in desk III exhibit that the bias voltage at 0.7 V shouldn't be a good choice for these scenes. Nonetheless, including a 2d bias voltage at 0.6 V to the 2nd set (leading to our third bias voltage set) improves the classification as proven through the thematic maps in third column (a-c) in Fig. 8. Sooner or later, the thematic maps in the final column in Fig. 8 (a-c) and and the classification error in desk III indicate practically ultimate classification results for the fourth set of bias voltages, i.E., when all ten biases are used.

Thematic maps and classification mistakes for the rock classification situation are proven in Fig. Eight (d) and Fig. 9, and table IV, respectively. For the granite-limestone-MW2 classification main issue we use 4 exclusive sets of bias voltages defined as follows: (i) one bias at zero.4 V; (ii) one bias at zero.7 V; (iii) two biases at zero.Three and 0.4 V; and (iv) all ten biases in the range of 0.Three V to 1.2 V. The primary and the 2nd thematic maps in Fig. Eight (d) exhibit that the primary bias voltage set gives more accurate results than the second one, i.E., bias at 0.Four V is more potent for this scene content material than the bias at zero.7 V. Utilising the 0.33 bias-voltage set, which combines two biases at 0.Three V and nil.Four V, improves the classification accuracy compared to the first two instances (the 1/3 thematic map in Fig. Eight (d)). Additionally, from the fourth thematic map in Fig. 8 (d) we see that the third bias set offers outcome similar to those making use of the fourth bias set, i.E., when all ten DWELL FPA bands are used.

V. CONCLUSION

We now have presented two model-situated, spatio-spectral part detection algorithms, termed the SRC and ASRC algorithms. The SRC algorithm makes it possible for the detection of edges which can be because of both material alternate or intensity variation in scenes containing a prescribed set of substances. The ASRC algorithm is a specialised version of the SRC algorithm, geared toward detecting edges which might be as a result of a transformation in the fabric only. The ASRC goals to lower the detection of false edges as a result of unwanted alterations within the intensity.

Both algorithms make use of spectral library information to assemble a sparse, non-separable and 3D edge operator even as exploiting the notion of spectral ratio distinction. The suggested SRC side detector performs as good because the MCG part detector for moderately challenging edges, with the abilities of requiring less operation than that required by way of the MCG algorithm. However, for challenging imagery containing isoluminant edges, the SRC and ASRC part detectors outperform the MCG and HySPADE edge detectors by using a broad margin, as quantified by using the detection and false-alarm probabilities. This supplies a powerful validation of the efficacy of the spectral ratio distinction idea by means of showing that the usage of prefer band ratios can lead to trustworthy identification of weak edges within the presence of noise. Moreover, with a slight develop in the complexity the ASRC algorithm, which also includes classification-centered step, is ready of minimizing the false-alarm edges, outperforming the SRC, MCG and HySPADE algorithms.

REFERENCES

[1] C. A. Musca, J. Antoszewski, K. J.Winchester, K. K. M. B. D. S. A. J. Keating, T. Nguyen, J. M. Dell, L. Faraone, P. Mitra, J. D. Beck, M. R. Skokan, and J. E. Robinson, “Monolithic integration of an infrared photon detector with a mems-based tunable filter,” IEEE Electron Device Letters, vol. 26, Dec. 2005.

[2] N. Gupta, R. Dahmani, and S. Choy, “Acousto-optic tunable filter based visible- to near-infrared spectropolarimetric imager,” Optical Engineering,vol. 41, May 2002.

[3] R. Gonzalez and R. Woods Digital Image Processing, 2001 :Prentice-Hall

[4] J. Canny "A computational approach to edge detection", IEEE Trans. Pattern Anal. Mach. Intell., vol. 8, no. 6, pp.679 -698 1986 .

[5] I. Sobel and G. Feldman "3 isotropic gradient operator for image processing", 1968.

[6] P. Blomgren and T. F. Chan "Color TV: Total variation methods for restoration of vector valued images", IEEE Trans. Image Process., vol. 7, no. 3, pp.304 -309 1998

[7] L. Lucchese and S. K. Mitra "Color image segmentation: A state-of-the-art urvey", Proc. Ind. Nat. Sci. Acad., vol. 67, no. 2, pp.207 -221 2001

[8] X. Chen and H. Chen "A novel color edge detection algorithm in RGB color space", Proc. IEEE 10th ICSP, pp.793 -796 2010

[9] G. Sapiro "Color snakes", Comput. Vis. Image Understand., vol. 68, no. 2, pp.247 -253 1997

[10] B. Sandberg and T. F. Chan Logic operators for active contours on multi-channel images, pp.2 -12 2002 :Dept. Math., UCLA

[11] P. Bao, D. Zhang and X. Wu "Canny edge detection enhancement by scale multiplication", IEEE Trans. Pattern Anal. Mach. Intell., vol. 27, no. 9, pp.1485 -1490 2005